Water Density Effects on Homogeneous Water-Gas Shift Reaction Kinetics

Steven F. Rice,* Richard R. Steeper, and Jason D. Aiken

Combustion Research Facility, Sandia National Laboratories, MS-9052, P.O. Box 969, Livermore, California 94551-0969

Received: July 21, 1997; In Final Form: December 3, 1997

Several years ago, using ab initio calculations, Melius et al. examined an interesting pathway for the homogeneous gas-phase water-gas shift reaction. They predicted that an enhancement in the rate of this reaction occurs at high water density due to changes in the generation of formic acid as an intermediate. To investigate this possibility, we have examined the conversion of CO and H_2O to CO_2 and H_2 in the absence of a catalyst in supercritical water at conditions from 410 to 520 °C and 2.0−60 MPa. In these experiments, Raman spectroscopy produced in situ, real-time measurements of reaction rates in an optically accessible, constant-volume reactor. The most rapid homogeneous rate measured, at 59 MPa and 450 °C, corresponds to an effective first-order reaction rate constant of 0.0033 s^{-1}. The data show that the measured reaction rates increase far faster than linearly as water density is raised above 0.35 g/cm^3, and the pressure dependence of the rate constant indicates that the transition state is characterized by an unusually high negative volume of activation, $\Delta v^{\ddagger} = -1135$ cm^3/mol. These data provide strong evidence that this is not a simple gas-kinetic bimolecular reaction at conditions in the neighborhood of the critical density. Rather, the participation of extra water molecules in the structure of the transition-state complex results in a high-order rate dependence on water density. The data are analyzed within the context of a transition-state local density enhancement, expressed as a cluster number, ξ_{ts}, found to be approximately 15 molecules.

Introduction

The water-gas shift reaction has been a key process in the worldwide chemical industry for many years:

$$CO + H_2O \rightleftarrows CO_2 + H_2 \qquad (1)$$

However, in the absence of a catalyst, the reaction is very slow at accessible industrial temperatures. The commercial process is conducted catalytically at ambient or elevated pressure in one or two stages using a "high-temperature" catalyst at about 400 °C and "low-temperature" catalysts at 200 °C. The apparent catalytic activity for the high-temperature, catalyzed conversion of CO can be as high as 1.5 s^{-1} at 400 °C with fresh catalyst and shows a weak, but positive, dependence on pressure.[1,2] However, these catalysts, especially the lower temperature system used for high conversion, can show severe effects of degradation due to poisoning by heteroatoms.[3] Recently, the water-gas shift reaction has also been explored by Elliott et al. in a two-phase system using high-temperature, pressurized water and alkali metal salts as potentially more effective and robust homogeneous catalysts.[4] In that work, a mechanism is proposed based on the formation of formate ion as an intermediate. The rate constant of the uncatalyzed reaction reported by Elliott et al. in near-liquid density water at 400 °C is 1×10^{-5} s^{-1}. There is a wealth of literature focusing on the catalytic water-gas shift reaction involving oxides and more unusual forms of most of the transition elements; however, these studies are not especially relevant to the uncatalyzed reaction that is the focus of this paper.

Our interest in fundamental reactions in supercritical water has led to an examination of the effects that the near liquidlike densities of supercritical water could have on this process. Using an optically accessible, constant-volume, high-pressure reactor,[5] we have examined the conversion of CO and H_2O to CO_2 and H_2 in the absence of a catalyst in water at conditions from 410 to 520 °C and 2−60 MPa. The experimental measurements can be analyzed using a transition-state model for this reaction in supercritical water and the theory of local density enhancement in the neighborhood of the transition-state complexes.

Model Background

An important aspect of modeling elementary reactions in supercritical water is determining whether neighboring water molecules in the dense fluid participate in the reaction chemistry. It is possible that the presence of high-density water enables individual elementary reactions to proceed at rates that are significantly different from rates predicted by extrapolating from gas-phase expressions to higher pressure. In fact, there are a number of ways that water can affect the rate of a reaction under these conditions. In the case of the water-gas shift reaction, we are interested in whether the presence of water at high density can modify the energetics of a transition-state complex. Thus, for example, additional water molecules can be incorporated into the transition-state structure directly or act in concert to stabilize that complex through solventlike electrostatic forces. The formation of higher density clusters surrounding a solute in a supercritical mixture has received considerable attention over the past decade from both experimental and theoretical approaches and provides the framework for interpreting the pressure dependence of the water-gas shift reaction in supercritical water.

Several years ago, Melius et al.[6] conducted a theoretical investigation of the homogeneous, gas-phase water-gas shift mechanism. They suggested that, at sufficiently high water

* Corresponding author: Telephone (925) 294-1353; Fax (925) 294-2276; E-mail sfrice@sandia.gov.

S1089-5639(97)02368-2 CCC: $15.00
Published on Web 03/28/1998

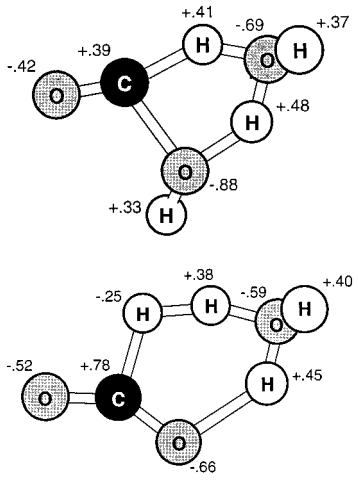

Figure 1. Transition-state geometries and charge distributions for CO + $2H_2O$ (top) and HCOOH + H_2O (bottom) from Melius et al.[6]

densities, the activation energies for CO conversion to formic acid and the subsequent decomposition of formic acid to CO_2 and H_2 are significantly reduced by the participation of additional water molecules in the transition-state complex.

$$\mathrm{CO} + n\mathrm{H_2O}\ (n = 2, 3) \rightarrow \mathrm{HCOOH} + (n-1)\mathrm{H_2O} \rightarrow \mathrm{CO_2} + \mathrm{H_2} + n\mathrm{H_2O} \quad (2)$$

Figure 1 (top) shows the transition-state structure for the formation of formic acid from CO and two water molecules. Since the two hydrogen atoms in the product formic acid originate from different water molecules, the transition-state structure is less strained and has a reduced heat of formation. When the extra water molecule is not present, the structure is much more strained and requires more energy to form. There is another structure suggested, involving three water molecules, that provides even more stabilization. The calculated activation energies for the one-, two-, and three-molecule activated complexes are 61.7, 35.6, and 19.3 kcal/mol, respectively.

There are also water-assisted transition states for the decomposition of formic acid to CO_2 and H_2. The activation energies of these structures are significantly lower than the calculated 64 kcal/mol for the unassisted unimolecular decomposition. A complex including a single additional water molecule is shown in Figure 1 (bottom). Note that in this case, analogous to the formation of formic acid, the two hydrogen atoms that form the product hydrogen molecule do not both come from formic acid.

The proposed detailed structure of the transition state provided the means to calculate the thermodynamics of the reactants, transition state, and products in the supercritical fluid over a range of temperature and pressure conditions, leading to qualitative predictions of the variation in reaction rate with these state variables. The calculations implicitly explored the effect of neighboring water molecules on the overall system's thermodynamics using a Peng−Robinson equation of state (EOS) for dilute mixtures,

$$P = RT/(v - b) - a/(v^2 - 2bv - b^2) \quad (3)$$

Individual species' critical properties T_c, V_c, and acentric factors for the transition-state complexes were estimated using some simple rules and analogy to similar-sized species with similar dipole moments and atomic charge distributions. These were combined using the corresponding states mixing rules[7] to yield the *a* and *b* parameters in eq 3. This equation of state for water, with a dilute concentration of solute, provided the partial molar departure functions, μ_i^D, that represent the change in the molar Gibbs energy due to nonideal dense gas effects. These were then used to calculate the partial molar volume of activation, $\Delta v^{\ddagger}$, for the formation of the transition states described above, $[\mathrm{CO} + n\mathrm{H_2O}]^*$, through the relationship

$$\Delta v^{\ddagger} = RT(\partial \Delta G^{\ddagger}/\partial P) \quad (4)$$

In the thermodynamic formulation of transition-state theory, the rate constant, *k*, is expressed as

$$k = (k_b T/h) v^{\Delta \nu} \exp(-\Delta G^{\ddagger}/RT) \quad (5)$$

where v is the molar volume; $\Delta G^{\ddagger}$ is the difference in the Gibbs free energy between the reactants and the transition-state complex; $\Delta \nu$ is the change in the molecularity to form the activated complex; and k_b, h, and R are Boltzmann's, Planck's, and gas constants. This leads to an approximate expression for the pressure dependence of a reaction (omitting possible diffusional pressure effects and the linear temperature term in the preexponential factor)

$$\partial(\ln k)/\partial P \approx -\Delta v^{\ddagger}/RT \quad (6)$$

where $\Delta v^{\ddagger}$ is the volume of activation. For our analysis, the rate constant, *k*, is pseudo-first-order in CO conversion with units s^{-1}.

By examining the magnitude of the pressure dependence of a reaction, eq 6 yields information about transition-state structure. Melius et al. found large negative volumes of activation (≈ -1100 cm^3/mol) associated with the polar nature of the structures in Figure 1 at densities near the critical density of water. They calculated that at gaslike densities, <5.0 mol/L, and again at liquid densities, >50 mol/L, the magnitudes of $\Delta v^{\ddagger}$ and therefore $\partial(\ln k)/\partial P$ would be much smaller.

Prior to the calculation of Melius et al., others had been focused on interpreting the behavior of partial molar volumes of solutes in supercritical fluids, typically other than water, in the immediate neighborhood of the solvent's critical point.[8] These efforts identified that the partial molar volume of the solute at infinite dilution, v_2^{∞}, could be described by

$$v_2^{\infty} = v\beta n[(\partial P/\partial n_2)_{T,V,N}] \quad (7)$$

where β is the solvent isothermal compressibility, $-(1/v)(\partial v/\partial P)_T$. The extension of these concepts to reaction rates in supercritical fluids[9] by Johnston and Haynes showed that large changes in rates as a function of pressure could be found near the critical point of the dilute mixture. To calculate the magnitude of the rates, they evaluated $\Delta v^{\ddagger}$ in eq 6 using

$$\Delta v^{\ddagger} = v\beta n[(\partial P/\partial n_{\ddagger})_{T,V,N} - (\partial P/\partial n_r)_{T,V,N}] \quad (8)$$

where the subscripts ‡ and r refer to the reactant and the transition state. They showed that the very large negative volumes of activation in eq 8 followed the system's compressibility curve closely. Thus, a reacting system that exhibited a more attractive potential between the solvent and the transition state than between solvent and reactant would see an enhancement in the rate with pressure; moreover, this effect would be greatly amplified in the neighborhood of the solvent's critical point due to the near divergence of the isothermal compressibility. It has been shown in a number of supercritical systems that the reaction rate increases with pressure dramatically at reduced pressures $P_r \sim P_c$ and reduced temperatures in the range

$1.0 > T_r > 1.2$. This effect decreases at higher pressures as the supercritical solvent approaches liquidlike densities, and the compressibility approaches zero.

Debenedetti and co-workers[10,11] created a classification scheme for solutes in supercritical fluids describing them as repulsive, weakly attractive, or attractive, based on the strength of the solute−solvent interaction. The relationship

$$v_2^{\infty}\rho = \rho RT\beta - \xi_c \tag{9}$$

was developed and provides an explicit form to connect the infinite dilution solute partial molar volumes to the Eckert clustering concept. In this expression, ξ_c is a cluster number, defined as the excess number of solvent molecules (relative to the bulk density) surrounding an infinitely dilute solute molecule. They have also investigated the effect of solute−solvent size asymmetry and showed that attractive behavior exists at reduced temperatures as high as 1.7 along the critical isochore.[12]

Since the infinite dilution partial molar volume of activation, $\Delta v^{\ddagger\infty}$, is the difference of the partial molar volumes of the transition state and the reactants, eq 9 becomes

$$\Delta v^{\ddagger\infty}\rho = \rho(v_{ts}^{\infty} - v_{co}^{\infty}) = \xi_{co} - \xi_{ts} \tag{10}$$

for the reaction considered here.

Subsequent to these developments, there have been a number of attempts to employ molecular dynamics (MD) simulations in Lennard-Jones supercritical solvents, which have shown clear evidence of the clustering effect.[13,14] The development of improved MD simulations of pure supercritical water has enabled MD simulations of ions,[15] ion pairs,[16] and organic molecules[17] in supercritical water, although not without uncertainty due to computational limitations on the system size. These calculations have shown the presence of local density enhancement of as many as 7−8 water molecules surrounding a sodium chloride ion pair. Cui and Harris[16] also show that the clustering effect extends to temperature and pressure conditions beyond the immediate vicinity of the critical point.

There is no data available on the EOS behavior of carbon monoxide in supercritical water. However, carbon monoxide has only a very small dipole moment, and its critical properties are nearly the same as isoelectronic N_2. Franck and co-workers have generated a wealth of data on the molar volumes of small molecules, including N_2, in supercritical water.[18] From these data and others, Gallagher et al.[19] have developed an equation of state for the water−N_2 system and have shown that the excess partial molar volume of N_2 in supercritical water is positive, fitting into the "repulsive" classification of Debenedetti. At 40 MPa and 407 °C, they report an infinite dilution partial molar volume of $v_2^{\infty} = 0.312$ L/mol. Using eq 9 with $\rho = 27.3$ mol/L and $\beta = 0.020$, we obtain $\xi_c = -7.7$; at 30 MPa, with density very near ρ_c, we get $\xi_c = -16.6$. An examination of this behavior over the entire range of conditions in this paper reveals that the solvent surrounding N_2, and by analogy probably CO, has a local density that is reduced relative to the bulk density.

The theoretical developments presented above enable the interpretation of the pressure dependence of the water-gas shift reaction in high-pressure steam and supercritical water. In particular, there are transition-state complexes of CO plus more than one water molecule that have reduced gas-phase activation energies, enabling the reaction to occur in the absence of metal catalysts or oxygen. These transition states correspond to three-body and even four-body collisions and will be difficult to form from a collision frequency standpoint at low water densities. However, as the density of the fluid is increased, we can expect these polar structures to be formed. The theory of clustering in the neighborhood of dilute solutes in supercritical fluids has established that local density enhancement is likely in such a system and that the clustering around the transition state will result in an increase in the reaction rate with pressure at conditions near the critical density. Furthermore, this pressure dependence can be interpreted in terms of a volume of activation that gives a measurement of the cluster number. This clustering can persist well above the critical temperature, but as the density of the system is raised above the critical density by increasing pressure, the pressure dependence will roll off as the bulk density approaches the cluster density.

Experimental Methods

We have employed Raman spectroscopy as an in-situ, real-time diagnostic for measuring reaction rates. This diagnostic permits the continuous monitoring of CO, CO_2, and H_2 concentrations as the reaction proceeds. The equipment used for these experiments and the concentration calibration methods are described in detail elsewhere.[5] Due to shorter reaction time scales encountered in the measurements presented here, we were compelled to install a mechanical stirrer to reduce the batch mixing time. Similar to other mechanically actuated, high-pressure feedthroughs,[20] the stirrer uses a packed valve stem design with dimensions similar to Autoclave Engineers, Inc., high-pressure valves. The shaft is driven by a variable-speed electric motor and is operated at approximately 200 rpm during injection in a typical experiment. The horseshoe-shaped paddle is designed so that when positioned vertically, it does not interfere with the input laser beam or the scattered light collection.

Our procedure begins with a calibration that relates the integrated Raman intensity of an individual pure species to a concentration calculated from a measured pressure of approximately 1.4 MPa. The high-pressure optical cell is then evacuated and refilled with water at the desired temperature and at a pressure slightly lower than the desired experimental value. Enough CO to yield a 0.15 mol/L mixture at the desired pressure is then rapidly injected over a period of 5 s while stirring vigorously—sufficient time to thoroughly mix the reactor contents. The mixtures are all quite dilute with respect to CO, with the mole fraction of CO being about 1% for the data taken near the critical density of water. By analogy to nitrogen−water mixtures, where the phase behavior is well-known, the mixture is in the single-phase region at all compositions above 660 K and pressures below 250 MPa.[18]

Raman spectra of the CO resonance at 2170 cm^{-1} are recorded every 10 s for the faster (higher pressure) reactions or every 30 s at conditions when the reaction is slower. Many of the individual experiments also include periodic measurements of the production of H_2 and CO_2. The Raman features used to measure these two species are centered at 4160 and 1388 cm^{-1}, respectively. In the case of CO_2, the Raman feature is the high-energy component of the Fermi dyad and is complicated with transition intensity being distributed over the fundamental and several hot bands. We have measured the integrated intensity of the entire feature over the experimental pressure range and have found that it changes very little as a function of water density. The hydrogen Q-branch is fully rotationally resolved at the lower pressures used here but has collapsed to a single feature at the highest pressures. In this case, the integrated intensity of the entire feature changes about 30% over the experimental pressure range.

Pressure was measured using low-pressure and high-pressure transducers for the calibration and kinetic runs, respectively.

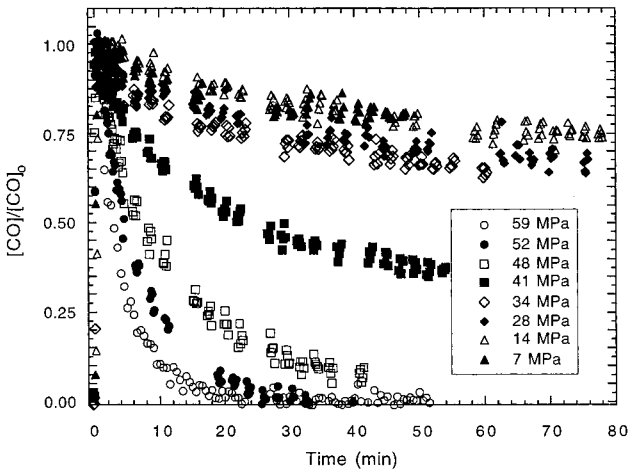

Figure 2. Observed concentration of CO reacting in supercritical water at 450 °C for a range of pressures. All the data were recorded with an initial CO concentration of approximately 0.15 mol/L H_2O.

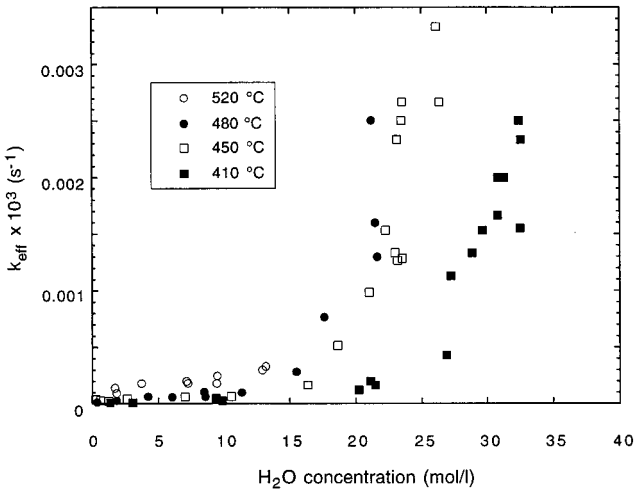

Figure 3. CO conversion rate constants vs water concentration at four experimental temperatures.

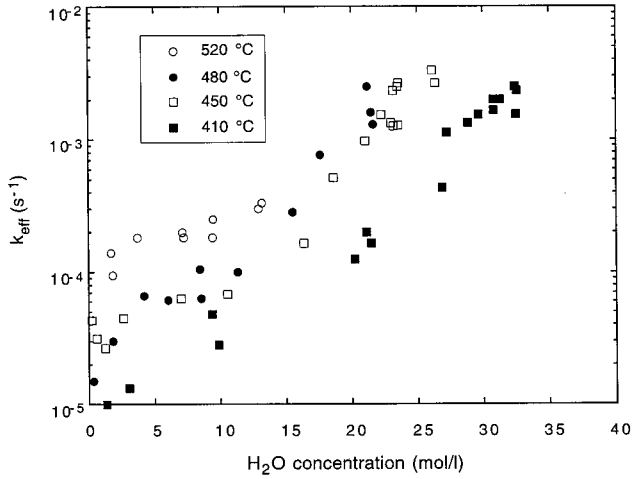

Figure 4. The data in Figure 3 replotted on a semilog plot.

The reaction runs were carried out at constant volume, not pressure. A small pressure increase (0.1−0.5 MPa) was measured over the course of the reaction. Because the mole fraction of CO was always small compared to the water concentration, the equation of state for water[21] alone was used to calculate water concentrations in the figures below. No correction was made for the small change in total molar volume due to the nonidealities of CO dissolution.

Results and Discussion

Figure 2 shows the results of kinetics experiments conducted for a range of total pressures at 450 °C. Attempts to fit the higher pressure data to a first-order expression were generally successful. However, the data, especially at lower pressure (<35 MPa), show initially a faster reaction rate, consuming about 10−20% of the CO, followed by a rate that is as much as a factor of 2 slower. To test the hypothesis that the faster data may indicate a surface-catalyzed reaction, we estimated the catalysis effect. Using our data at 48 MPa and 450 °C as a typical "fast" reaction, $k_{eff} = 9.8 \times 10^{-4}$ s^{-1}, and estimating the surface area of the reactor to be 10 cm^2, we calculate a catalytic activity for the reactor surface of 2.2×10^{-8} mol/(cm^2 s atm). As discussed in the Introduction, the catalyzed water-gas shift process has an apparent rate of 1.5 s^{-1}. Ruthven[2] has reexpressed this as an intrinsic catalyst activity, k_s, approximately equal to 2×10^{-10} mol/(cm^2 s atm) at 400 °C. It is unlikely that our reactor surface is 2 orders of magnitude more active than a commercial shift catalyst, ruling out the possibility of surface-catalyzed reaction dominating the observations in these experiments.

The initial rapid loss of CO at lower pressures indicates that the reaction mechanism is more complicated than a simple first-order process. In fact, the model presented by Melius et al. suggests that the two steps, formation and decomposition of formic acid, may have comparable rate constants. At higher pressures, the carbon balances are generally good (within the approximately ±5% measurement accuracy), while at lower pressures there is a deficit of carbon (as much as 20%) for early times as measured by the sum of the CO and CO_2 concentrations. However, no intermediates have been spectroscopically identified. We attempted to measure directly the decomposition of formic acid in supercritical water in this temperature and pressure range and found that complete conversion to CO_2 occurred within 10 s, i.e., within the time scale of injection. Since no intermediates could be observed and carbon balances were generally good especially at the higher pressures most relevant to this work, the evidence suggests that the rate-limiting step in this two-step model is the formation of formic acid and not the subsequent decomposition to H_2 and CO_2.

For analysis purposes, we have chosen to discard the early data points in the lower pressure measurements and fit a first-order reaction rate to the subsequent later-time data. However, this is the primary source of uncertainty in the data. All of the experiments produced at least some variation in the fitted rate constant, depending on the length of time discarded at beginning of the reaction or the duration of the individual data run. Although the statistical error in the fits was typically less than 3%, the lack of precise first-order kinetics produces considerable scatter in the data. At low pressures, seen in the figures presented below, this amounts to an error of as much as a factor of 2 in the rate constant.

Figure 3 shows a plot of our complete set of measurements evaluated using first-order rate constants, k_{eff}, expressed as

$$d[CO]/dt = -k_{eff}[CO] \qquad (11)$$

This form of rate data reduction is often used to characterize catalyzed industrial processes. Figure 4 shows the same data on a semilog plot. The effective first-order reaction rate constants conclusively show a strong water density dependence over the entire concentration range examined.

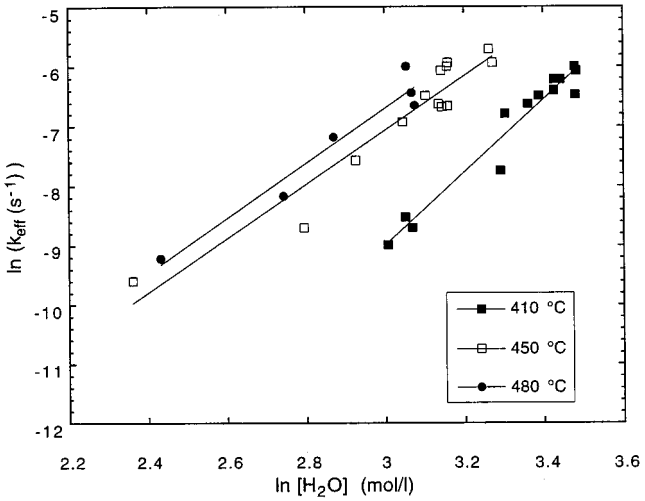

Figure 5. The data in Figure 3 at high water density replotted on a log−log plot. The lines are the results of linear least-squares fits to the data.

Evaluating the Arrhenius expression for k_{eff},

$$k_{eff} = A \exp(-E_a/RT) \tag{12}$$

at a water concentration of 20 mol/L produces $A = 10^{7.22\pm2.6}$ s^{-1} and $E_a = 34.7 \pm 8.6$ kcal/mol. This effective activation energy agrees well with the water-assisted activation energy obtained in the calculation for the transition state shown in Figure 1. However, as is pointed out by Melius et al.,[6] there are competing effects in this system as temperature is raised. In addition to water's direct role in the activated complexes in Figure 1, significant stabilization can originate from the structure of surrounding water molecules.

An alternative expression for the rate can be written as

$$d[CO]/dt = -k'[CO]\,[H_2O]^a \tag{13}$$

where $k_{eff} = k'[H_2O]^a$. A possible interpretation of water's role can be viewed by plotting ln(k_{eff}) vs ln(H_2O) to yield straight lines for the different temperatures, with slopes representing the molecularity of the water dependence. Figure 5 shows this plot using the data taken at 410, 450, and 480 °C at densities above 10 mol/L. The resulting fitted values of the exponent, a, are 6.1 ± 0.42, 4.5 ± 0.41, and 4.6 ± 0.55, respectively. It seems unlikely that as many as 4−6 water molecules participate directly in the transition-state structure, and thus the global rate expression does not truly represent the molecularity of the molecular-scale transition state. We would expect smaller values (1 or 2) if the gas-phase transition-state model stabilization presented by Melius were the only factor affecting the dependence on water concentration. The larger values for the exponent suggest that the dependence on water concentration is not as simple as a well-defined gaseous transition state, and another interpretation of the pressure dependence of the reaction is needed.

The model presented by Melius et al. predicts that the $\Delta v^{\ddagger}$ of this reaction varies greatly with the density of the supercritical fluid. At conditions near the critical density (29.5 MPa, 427 °C, $\rho = 0.19$ g/cm^3, for example), the $\Delta v^{\ddagger}$ is calculated to be −1178 cm^3/mol for the transition state in Figure 1 (top). This is much greater than typical liquidlike values for known pressure-dependent reactions (no greater than −50 cm^3/mol[22]). At low density, where an ideal-gas equation of state is adequate, only a small $\Delta v^{\ddagger}$ is predicted. Likewise, at higher pressure and near liquid conditions (98.6 MPa, 427 °C, $\rho = 0.65$ g/cm^3), a modest value of −119 cm^3/mol is predicted.

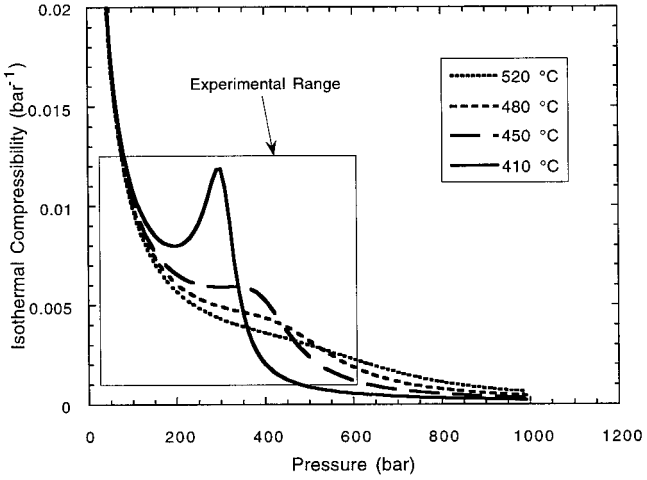

Figure 6. Isothermal compressibility of water in the pressure and temperature range accessed in the experiments.

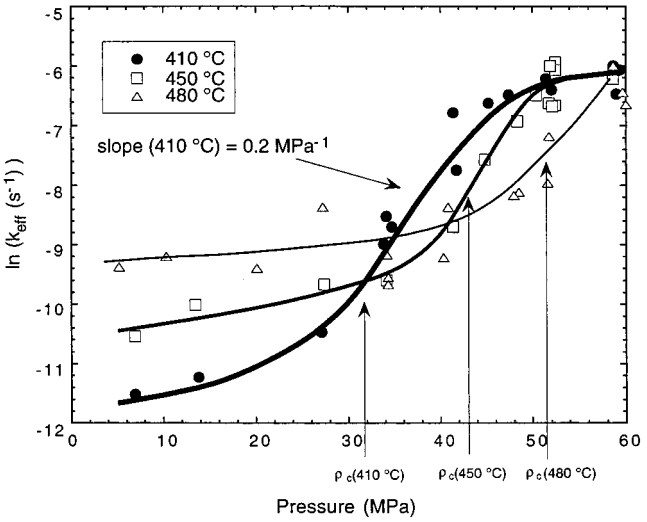

Figure 7. Pressure dependence of the rate constant at 410, 450, and 480 °C. The fit to the steepest part of the data at 410 °C is centered at approximately 36 MPa and $\rho = 0.42$ g/cm^3.

Figure 6 shows the compressibility of water over the experimental range. These experiments have been conducted over a sufficiently broad pressure range to span the critical isochore for 410−480 °C. Although data near the critical point were not obtained, the experiments sampled the region described by Petche and Debendetti that corresponds to the system having the potential for attractive interaction and therefore significant local density enhancement. The low concentration of reactants and products will not measurably affect the compressibility of the mixture.

Figure 7 shows the data in Figure 3 plotted vs pressure. The widest density range belongs to the set at 410 °C which extends to 0.6 g/cm^3. The slope of the curve goes through a maximum at about 36 MPa; by fitting the 20−50 MPa range to a line, we obtain $\partial(\ln k)/\partial P = 0.2 \pm 0.020$ MPa^{-1}. Inserting this into eq 6 results in a value of $\Delta v^{\ddagger} = -1135 \pm 113$ cm^3/mol. Note that at higher density the slope decreases. This is in excellent agreement with the model's prediction. The higher temperature curves at 450 and at 480 °C show their maximum slopes at higher total pressures, with all three maximum slopes occurring near the critical density.

Using this value of $\Delta v^{\ddagger}$ and an estimate of CO partial molar volumes in supercritical water, v_{co}^{∞}, eqs 9 and 10 permit us to calculate the transition-state cluster number, ξ_{ts}. Since there is no *PVT* data available for CO in supercritical water, we are forced to use nitrogen data to obtain an estimate of CO partial molar volumes in supercritical water. This is done with some reservation since CO does have a small dipole moment and is not likely to be as repulsive as N_2. For instance, using the EOS in Melius et al. at 300 atm and 700 K, v_{co}^{∞} is +585 cm^3/mol. The corresponding result from the NIST EOS for nitrogen is +673 cm^3/mol at 30 MPa and 700 K. Given the uncertainy in v_{co}^{∞} at 36 MPa and 410 °C, we will use a value of 500 cm^3/mol as a rough estimate, which yields $\xi_{co} = -9.2$ from eq 9. Inserting this value and the experimental $\Delta v^{\ddagger}$ above at 36 MPa and 410 °C into eq 10 yields $\xi_{ts} = 15.5$. The same calculation can be done at 480 °C. The maximum slope in Figure 7 is approximately 0.15 MPa^{-1} at 50 MPa and $\Delta v^{\ddagger} = -935$ cm^3/mol. With v_{co}^{∞} (750 K, 50 MPa) $\leq$ 360 cm^3/mol (from NIST tables for nitrogen), we obtain $\xi_{co} \geq -4.4$, such that $\xi_{ts} \leq 11.1$. Expressing this as an upper limit results from the estimate of $v_{co}^{\infty} \leq 360$ cm^3/mol as an upper limit for CO. Thus, the cluster numbers do decrease as the temperature increases beyond T_c but still remain significant at $T_r = 1.15$. These results agree with theoretical predictions.[16,12]

In the thermodynamic interpretation of activated complex theory, the empirical activation energy, E_a, determined above to be 34.7 kcal/mol, can be interpreted as $\Delta H^{\circ\ddagger}$ from

$$k_f = k_b T/h \exp(-\Delta G^{\circ\ddagger}/RT) \quad (14)$$

and

$$\Delta G^{\circ\ddagger} = \Delta H^{\circ\ddagger} - T\Delta S^{\circ\ddagger} = \Delta E^{\circ\ddagger} + P\Delta V^{\circ\ddagger} - T\Delta S^{\circ\ddagger} \quad (15)$$

where $\Delta G^{\circ\ddagger}$, $\Delta H^{\circ\ddagger}$, $\Delta S^{\circ\ddagger}$, $\Delta E^{\circ\ddagger}$, and $\Delta V^{\circ\ddagger}$ are the thermodynamic quantities of activation for free energy, enthalpy, entropy, internal energy, and volume. The observed E_a of 34.7 kcal/mol is composed of the $P\Delta V^{\circ\ddagger}$ term and the gas-phase term from the ab initio calculations where $P\Delta V^{\circ\ddagger}$ equals approximately −10 kcal/mol at 40 MPa and $\Delta V^{\circ\ddagger} = -1 \times 10^3$ cm^3/mol. This results in an energy of activation, $\Delta E^{\circ\ddagger}$, of about 25 kcal/mol, which is in the neighborhood of the ab initio values calculated in Melius et al. for one and two additional water molecules in the activated complex for the formation of formic acid.

Conclusions

A theoretical analysis of the water-gas shift reaction in supercritical water led Melius et al. to predict that densities approaching the critical density of water afford a change in the energetics of the homogeneous water-gas shift mechanism that could result in greatly increased conversion rates in a catalyst-free environment. The results from the experimental work presented in this paper on the water-gas shift reaction in supercritical water show that a modest increase in operating temperature and an increase in system pressure to 60 MPa produces conversion rates significantly accelerated from the low-pressure rate in the absence of a catalyst. However, the rate remains much slower than the industrial catalyzed process. The experimental parameters describing this change in energetics are in good agreement with the model. The interpretation of these data within the context of an increase in the local density of the supercritical solvent is in good agreement with the view that significant clustering can occur at temperatures significantly higher than T_c. The data support the theoretical prediction of the existence of a polar transition-state complex, characterized by an unusually large negative volume of activation, that results from a dramatic change in the local density of the supercritical fluid.

Acknowledgment. This work was supported by the DoD/DOE/EPA Strategic Environmental Research and Development Program (SERDP). We wish to thank Carl Melius and Dave Ross (SRI International) for valuable discussions.

References and Notes

(1) Moe, J. M. *Chem. Eng. Prog.* **1962**, *58*, 33−36.
(2) Ruthven, D. M. *Can. J. Chem. Eng.* **1969**, *47*, 327−331.
(3) Hawker, P. N. *Hydrocarbon Process.* **1982**, 183−187.
(4) Elliot, D. C.; Selaock, J. L. J. *Ind. Eng. Chem. Prod. Res. Dev.* **1983**, *22*, 426−431.
(5) Steeper, R. R.; Rice, S. F.; Kennedy, I. M.; Aiken, J. D. *J. Phys. Chem.* **1996**, *100*, 184−189.
(6) Melius, C. F.; Bergan, N. E.; Shepherd, J. E. *Proceedings of the Twenty-Third Symposium (International) on Combustion*; The Combustion Institute: Pittsburgh, PA, 1990; pp 217−223.
(7) Reid, R. C.; Prausnitz, J. M.; Poling, B. E. *The Properties of Gases and Liquids*, 4th ed.; McGraw-Hill: New York, 1987.
(8) Eckert, C. A.; Ziger, D. H.; Johnston, K. P.; Kim, S. *J. Phys. Chem.* **1986**, *90*, 2738−2746.
(9) Johnston, K. P.; Haynes, C. *AIChE J.* **1987**, *33*, 2017−2026.
(10) Debenedetti, P. G. *Chem. Eng. Sci.* **1987**, *42*, 2203−2212.
(11) Debenedetti, P. G.; Mohamed, R. S. *J. Chem. Phys.* **1989**, *90*, 4528−4536.
(12) Petsche, I. B.; Debenedetti, P. G. *J. Phys. Chem.* **1991**, *95*, 386-399.
(13) Wu, R.-S.; Lee, L. L.; Cochran, H. D. *Ind. Eng. Chem. Res.* **1990**, *29*, 977−988.
(14) Petsche, I. B.; Debenedetti, P. G. *J. Chem. Phys.* **1989**, *91*, 7075−7084.
(15) Cummings, P. T.; Cochran, H. D.; Simonson, J. M.; Mesmer, R. E.; Karaborni, S. *J. Chem. Phys.* **1991**, *94*, 5606−5621.
(16) Cui, S. T.; Harris, J. G. *Chem. Eng. Sci.* **1994**, *49*, 2749−2763.
(17) Cummings, P. T.; Chialvo, A. A.; Cochran, H. D. *Chem. Eng. Sci.* **1994**, *49*, 2735−2748.
(18) Japas, M. L.; Franck, E. U. *Ber. Bunsen-Ges. Phys. Chem.* **1985**, *89*, 793−800.
(19) Gallagher, J. S.; Levelt Sengers, J. M. H.; Abdulagatov, I. M.; Watson, J. T. R.; Fenghour, A. NIST Report #1404, 1993.
(20) Costantino, M. *Rev. Sci. Instrum.* **1991**, *62*, 1668−1669.
(21) Haar, L.; Gallagher, J. S.; Kell, G. S. *NBS/NRC Steam Tables: Thermodynamic and Transport Properties and Computer Programs for Vapor and Liquid States of Water in SI Units*; Hemisphere Publishing Corporation: New York, 1984.
(22) Isaacs, N. S. *Liquid Phase High Pressure Chemistry*; Wiley and Sons: New York, 1981.